Electron delocalization on iron sites in thallium and lead based ferrites $(Tl, Pb)Sr_3Fe_2O_8$ and $(Tl, Pb)Sr_4Fe_2O_9$: Mössbauer study

1996 J. Phys.: Condens. Matter 8 6297

(http://iopscience.iop.org/0953-8984/8/34/017)

J. Phys.: Condens. Matter **8** (1996) 6297–6312. Printed in the UK

Electron delocalization on iron sites in thallium and lead based ferrites $(Tl, Pb)Sr_3Fe_2O_8$ and $(Tl, Pb)Sr_4Fe_2O_9$: Mössbauer study

N Nguyen†, A Ducouret†, D Groult†, J M Grenèche‡ and B Raveau†

† Laboratoire CRISMAT, CNRS URA 1318, ISMRA, Université de Caen, 14050 Caen Cédex, France

‡ Laboratoire de Physique de l'Etat Condensé, CNRS URA 807, Université du Maine, 72017 Le Mans Cédex, France

Received 22 April 1996

Abstract. A Mössbauer study on powder samples of the two series of iron based oxides $ASr_3Fe_2O_8$ and $ASr_4Fe_20_9$ where A is a $5d^{10}$ cation ($A = Tl^{3+}, Pb^{4+}, Hg^{2+}$) is reported. In both families, the thermal evolution of the Mössbauer spectra associated with susceptibility measurements provides evidence for a mixture of high-spin localized Fe^{3+} and Fe^{4+} at low temperature and of different mixed valence states at higher temperatures, which are interpreted in terms of a dynamical electron delocalization. The number of intermediate-valence iron sites observed by Mössbauer spectroscopy depends on the magnitude of the hopping frequency with respect to the characteristic ^{57}Fe Mössbauer frequency. This process, governed by both the temperature and the mean charge of the A cations, is also demonstrated by the electronic conductivity measurements. Because of the low dimensionality of the structure, O_9 compounds allow the electron delocalization to start at lower temperatures than in the O_8 family.

1. Introduction

Recently two series of layered iron oxides $(Tl, Pb, Hg)Sr_4Fe_2O_9$ [1–4] and $(Tl, Pb)Sr_3Fe_2O_8$ [5, 6] were discovered. These phases, whose structures derive from perovskite intergrowths, are closely related to the superconducting cuprates, particularly as their bidimensional character is enhanced by the tendancy of iron to exhibit a '$5+1$' coordination, i.e. distorted octahedral or almost regular pyramidal, in these materials. Thus, the $(Tl, Pb, Hg)Sr_4Fe_2O_9$ series is isostructural with the '1201–0201' cuprate $TlBa_2La_2Cu_2O_9$ [7]: the structure consists of an intergrowth of single octahedral perovskite layers with double and single rock salt layers (figure 1(a)). The $(Tl, Pb)Sr_3Fe_2O_8$ oxides are related to the '1212' cuprates $(Tl, Pb)Sr_2CaCu_2O_{7-\delta}$ [8, 9]; they correspond to an intergrowth of double perovskite layers with double rock salt layers (figure 1(b)).

Non-stoichiometry phenomena, involving both oxygen and $5d^{10}$ cations (Tl, Hg or Pb), occur in these oxides so that various valence states are observed for iron, depending on the method of synthesis of those phases. The most important issue that has not been answered to date for these materials deals with the electronic distribution on the 'Fe–O' framework, which may appear controversial by comparing the results of the different

0953-8984/96/346297+16$19.50

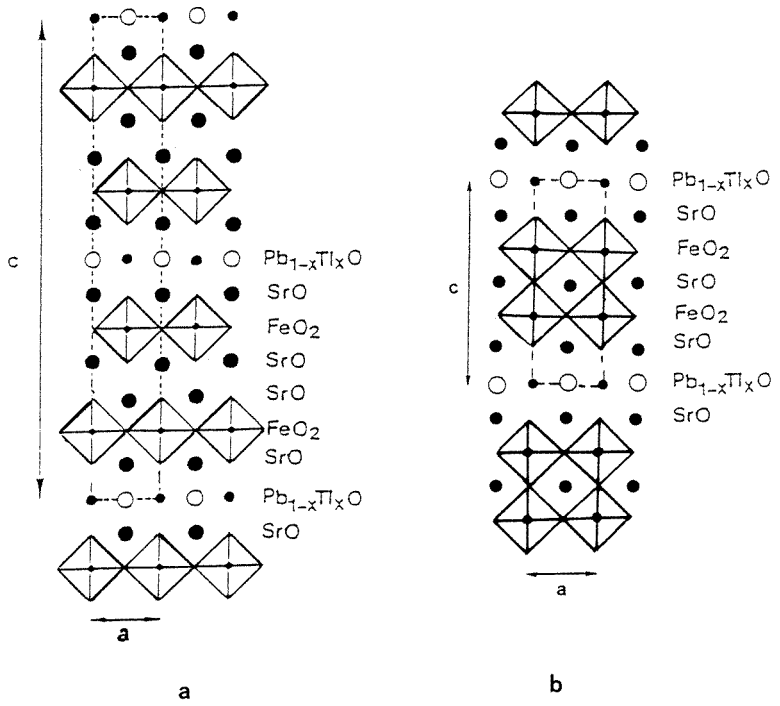

Figure 1. Schematic drawings of the intergrowth structures of the (Tl, Pb, Hg)$Sr_4Fe_2O_9$ (a) and (Tl, Pb)$Sr_3Fe_2O_8$ (b) series.

authors. For instance the 4.2 K Mössbauer spectra of the 'O_8' oxides—$TlSr_3Fe_2O_8$ [5] and $Tl_{0.5}Pb_{0.5}Sr_3Fe_2O_8$ [6]—were interpreted as a disproportionation of iron, leading to the existence of localized Fe^{3+} and Fe^{4+} species at low temperature, whereas for the 'O_9' oxide $TlSr_4Fe_2O_9$ a mixture of Fe^{3+} and $Fe^{3.75+}$ was proposed [10].

For other compositions, only room-temperature (RT) Mössbauer spectra were registered. The dispersion of the quadrupole splitting (QS) values at RT have provided evidence for various local environments of iron, in contrast to the crystallographic results that suggested only one iron site. This complex behaviour, involving several Fe sites, was explained thanks to electrical field gradient (EFG) calculations, by a variation of the apical oxygen position of the distorted FeO_6 octahedra, induced by a change of the coordination of the $5d^{10}$ cation. Nevertheless, for the same compound, a large dispersion of the isomer shift (IS) values at 293 K was observed from one site to the other; this has not yet been clearly interpreted.

In order to answer these questions, a recapitulative Mössbauer study, performed on 'O_8' and 'O_9' oxides at various temperatures was absolutely necessary. The present detailed study, carried out on Tl '1201–0201' and Tl '1212' type ferrites, allows a better understanding of the valence states of iron, as well as of electron transfer mechanisms occurring during temperature variations in these materials. Relationships between structure, magnetism and electron transport properties are also studied.

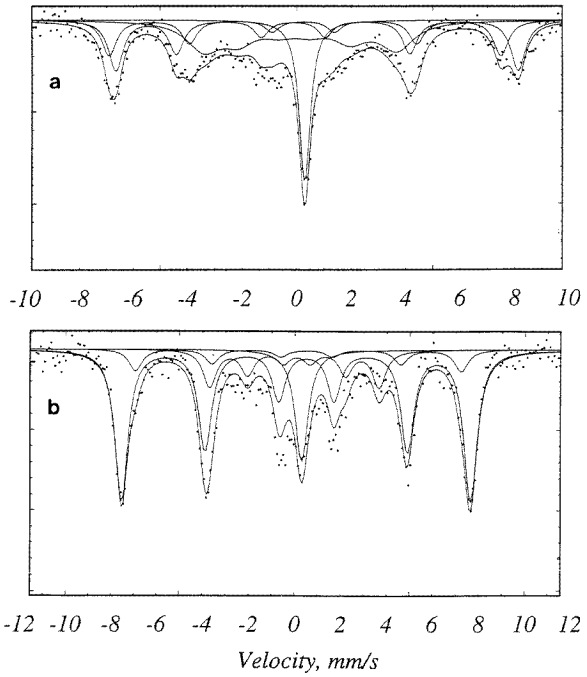

Figure 2. Mössbauer spectra at 4.2 K of $TlSr_3Fe_2O_8$ (a) and $Tl_{0.5}Pb_{0.5}Sr_3Fe_2O_8$ (b).

2. Experimental details

As mentioned above, the oxygen and cation (Tl, Hg, Pb) stoichiometries depend on the experimental conditions, so it is difficult to compare the results obtained by two different authors for a same phase. In order to ensure the coherence of the results, we have systematically performed new synthesis for all the compounds of the two O_8 and O_9 families. Their structural characteristics and the A and O stoichiometries were established by energy dispersive spectroscopy (EDS), X-ray and neutron diffractions and also by chemical titration of the oxygen content. These methods and sample synthesis have been described elsewhere [1–6]. Indeed for the same nominal composition, small deviations both in the metal (Tl, Hg, Pb) and in the oxygen stoichiometries could appear from one synthesis to another. Therefore, small differences may be eventually observed between the Mössbauer fitted results reported in this work and those previously reported [1–3, 5], but in this way an accurate comparison of the behaviour of each compound at each temperature can be made.

Mössbauer absorption powder spectra were recorded at various temperatures using a conventional spectrometer with a $^{57}Co/Rh$ source. The spectra obtained were least-squares fitted using the computer program MOSFIT [11].

Isomer shift values are quoted relative to metallic α-iron at 293 K. In the present study, Lamb–Mössbauer f-factors were assumed to be the same for the different iron sites, whatever the temperature.

The electronic conductivity of the samples was measured on sintered powder bars by means of a standard four-probe method. The susceptibility measurements were recorded with a Faraday balance from 5 K to 800 K.

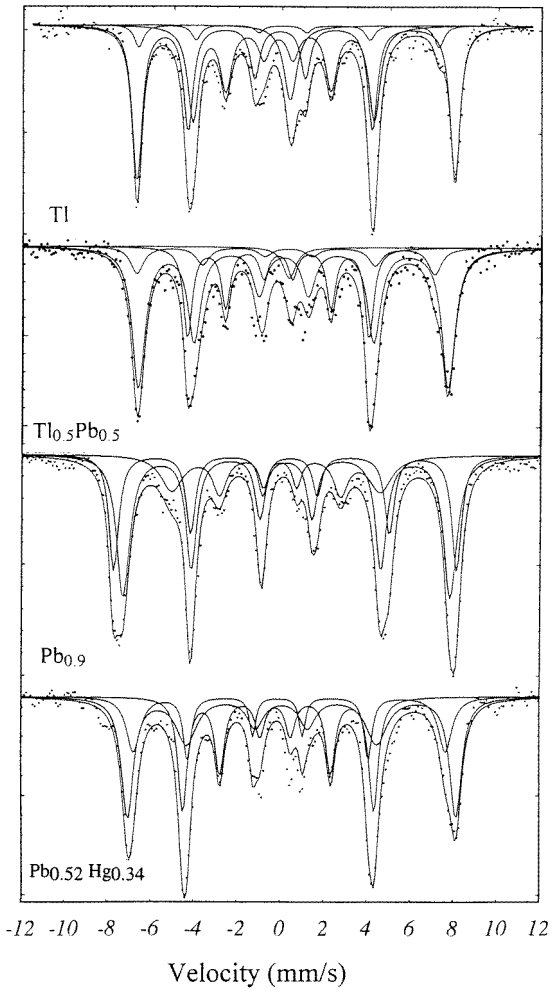

Figure 3. Magnetic Mössbauer spectra at 4.2 K of the (Tl, Pb, Hg)$Sr_4Fe_2O_9$ oxides.

3. Results and discussion

3.1. Mössbauer data at 4.2 K

Figures 2 and 3 show the 4.2 K magnetic spectra of the O_8 and O_9 series respectively. One can observe that the iron ions are not yet well magnetically ordered in $TlSr_3Fe_2O_8$ (figure 2(a)) at low temperature. All spectra can be systematically fitted (tables 1 and 2) with three main components: two components, denoted A_1 and A_2, with 0.27 mm s^{-1} < IS < 0.46 mm s^{-1} and the hyperfine field H_f lying in the range 42.6 T < H_f < 49.2 T, and one, denoted B, with -0.04 mm $s^{-1} \leqslant$ IS $\leqslant$ 0.14 mm s^{-1} and 22 T $\leqslant H_f \leqslant$ 29.9 T. The IS and H_f values of A_1 and A_2 sites are typical of high-spin localized Fe^{3+}; those of the B site correspond to $S = 2$ localized Fe^{4+} [12]. An additional reason for the assignment of the B site to Fe^{4+} will be given below.

Table 1. Fitted hyperfine Mössbauer parameters for $ASr_3Fe_2O_8$-type oxides (A = Tl, Pb).

A composition	T (K)	Site	Fe charge	IS (mm s^{-1}) (∓0.02)	2ϵ[a] (mm s^{-1}) or QS[b] (mm s^{-1}) (∓0.02)	H_f (T) (∓0.02)	(%) (∓5)
Tl	4.2	A_1	3	0.42	0.87	45.9	28
		A_2	3	0.38	0.06	44.7	20
Mean A		B	4	0.13	0.22	22.0	35
charge = 2.85		D	3	0.41	0.00	—	17
	293	A'_1	3	0.29	0.89	—	47
		A'_2	3	0.31	0.39	—	9
		B′	4	0.01	0.47	—	34
		D	3	0.35	0.00	—	10
$Tl_{0.5}Pb_{0.5}$	4.2	A_1	3	0.39	−0.46	47.2	63
		A_2	3	0.44	−0.36	44.0	9
Mean A		B	4	0.14	−0.09	22.9	16
charge = 3.50		D	3	0.41	0.00	—	12
	150	A′	3	0.38	1.20	—	72
		B	4	0.03	0.52	—	23
		D	3	0.36	0.00	—	5
	180	A′	3	0.35	1.18	—	67
		C'_1	*m*	0.21	0.78	—	8
		C'_2	*n*	0.06	0.49	—	20
		D	3	0.31	0.00	—	5
	210	A′	3	0.33	1.15	—	63
		C'_1	*m*	0.21	0.90	—	14
		C'_2	*n*	0.06	0.54	—	17
		D	3	0.31	0.00	—	6
	240	A′	3	0.32	1.12	—	54
		C'_1	*m*	0.21	0.93	—	22
		C'_2	*n*	0.07	0.61	—	19
		D	3	0.31	0.00	—	5
	293	A′	3	0.27	1.01	—	53
		C'_1	*m*	0.18	0.92	—	20
		C'_2	*n*	0.09	0.76	—	18
		D	3	0.29	0.00	—	9
	400	A′	3	0.18	0.98	—	53
		C′	3.5	0.11	0.87	—	42
		D	3	0.23	0.00	—	5

[a] Quadrupole shift of the magnetic Mössbauer sites.
[b] Quadrupole splitting of the paramagnetic Mössbauer sites.

Besides these three iron sites, in some compounds, principally in the O_8 family, one observes a weak contribution of an additional Fe^{3+} site, denoted D, characterized by a single line with 0.41 mm $s^{-1} \leqslant$ IS $\leqslant$ 0.49 mm s^{-1}. The origin of this paramagnetic D site may be the existence of superparamagnetic iron oxide particles within the principal phase probably resulting from a lack of complete reaction during the synthesis.

According to the relative intensity (%) of the Mössbauer sites and to the cation composition determined by EDS analysis and from X-ray or neutron diffraction data, the oxygen stoichiometry could be evaluated and compared to that obtained from chemical analysis results. A good agreement was observed between the two series of measurements (table 3).

Table 2. Fitted hyperfine Mössbauer parameters for $ASr_4Fe_2O_9$-type oxides (A = Tl, Pb, Hg).

A composition	T (K)	Site	Fe charge	IS (mm s^{-1}) (∓0.02)	2ϵ[a] (mm s^{-1}) or QS[b] (mm s^{-1}) (∓0.02)	H_f (T) (∓0.02)	(%) (∓5)
Tl	4.2	A_1	3	0.38	0.74	45.7	50
		A_2	3	0.27	0.28	43.1	7
Mean A		B	4	0.06	0.24	26.0	35
charge = 2.94		D	3	0.48	0.00	—	8
	293	A'_1	3	0.23	0.69	—	32
		A'_2	3	0.22	0.62	—	15
		C'_1	*m*	0.14	0.54	—	19
		C'_2	*n*	0.18	0.36	—	34
$Tl_{0.5}Pb_{0.5}$	4.2	A_1	3	0.46	0.46	46.5	60
		A_2	3	0.38	−0.15	44.7	11
Mean A		B	4	−0.04	−0.01	27.2	26
charge = 3.50		D	3	0.49	0.00	—	3
	20	A_1	3	0.42	0.74	45.8	37
		A_2	3	0.38	0.09	42.6	36
		B	4	0.01	0.01	26.1	26
		D	3	0.49	0.00	—	1
	77	A'	3	0.38	0.97	—	53
		C'_1	*m*	0.22	0.88	—	12
		C'_2	*n*	0.19	0.20	—	35
	293	A'_1	3	0.23	0.79	—	51
		A'_2	3	0.24	0.20	—	4
		C'	3.5	0.17	0.68	—	45
$Pb_{0.9}$	4.2	A_1	3	0.43	−0.16	49.2	29
		A_2	3	0.38	0.03	46.9	50
Mean A		B	4	−0.02	−0.26	29.9	21
charge=3.60							
	293	A'_1	3	0.30	0.77	—	49
		A'_2	3	0.36	0.08	—	10
		C'	3.5	0.18	0.73	—	41
Pb	293	A'_1	3	0.27	0.82	—	29
Mean A		A'_2	3	0.22	0.69	—	71
charge = 4							
$Pb_{0.52}Hg_{0.34}$	4.2	A_1	3	0.43	0.46	47.0	48
		A_2	3	0.28	0.54	44.7	19
Mean A		B	4	−0.03	0.11	27.3	31
charge = 2.76		D	3	0.41	0.00	—	2
	293	A'	3	0.26	0.69	—	47
		C'_1	*m*	0.17	0.58	—	23
		C'_2	*n*	0.11	0.37	—	30

[a] Quadrupole shift of the magnetic site.
[b] Quadrupole splitting of the paramagnetic site.

3.2. Mössbauer data at 293 K

At this temperature, all the compounds exhibit a paramagnetic behaviour (figures 4 and 5) with electric hyperfine interactions corresponding to quadrupole splitting values QS up to 1 mm s^{-1}. One can distinguish two main types of iron sites (tables 1 and 2).

Table 3. Oxygen content per formula unit for $ASr_3Fe_2O_8$ and $ASr_4Fe_2O_9$-type oxides.

Compound	From chemical analysis (∓0.05)	From Mössbauer data at 4.2 K (∓0.05)
$TlSr_3Fe_2O_8$	7.85	7.85
$Tl_{0.5}Pb_{0.5}Sr_3Fe_2O_8$	8.00	7.91
$TlSr_4Fe_2O_9$	8.88	8.85
$Tl_{0.5}Pb_{0.5}Sr_4Fe_2O_9$	8.92	9.01
$Pb_{0.9}Sr_4Fe_2O_9$	8.95	9.01
$PbSr_4Fe_2O_9$	9.00	—
$Pb_{0.52}Hg_{0.34}Sr_4Fe_2O_9$	8.58	8.64

(i) A first type A′ with $0.22 \text{ mm s}^{-1} \leqslant \text{IS} \leqslant 0.36 \text{ mm s}^{-1}$, corresponding to well localized Fe^{3+} ($S = 5/2$) sites, is observed for every compound, composed of one A′ site in $Tl_{0.5}Pb_{0.5}Sr_3Fe_2O_8$ (figure 4(a), table 1) and $Pb_{0.52}Hg_{0.34}Sr_4Fe_2O_9$ (figure 5, table 2) or of two A'_1 and A'_2 components in the other compounds.

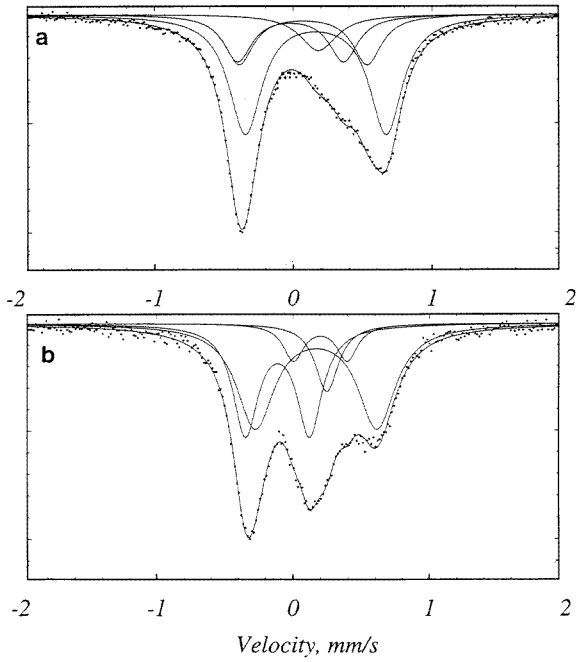

Figure 4. Mössbauer spectra at 293 K of $Tl_{0.5}Pb_{0.5}Sr_3Fe_2O_8$ (a) and $TlSr_3Fe_2O_8$ (b).

(ii) Except for $TlSr_3Fe_2O_8$, a second type of site (C′) is evidenced with weaker IS values ($0.09 \text{ mm s}^{-1} \leqslant \text{IS} \leqslant 0.18 \text{ mm s}^{-1}$) intermediate between those generally observed for high-spin localized Fe^{3+} ($\text{IS} \approx 0.22$ to 0.58 mm s^{-1}) and Fe^{4+} (-0.20 to 0.14 mm s^{-1}) at 293 K [13]. Because previous magnetic susceptibility measurements [3, 5] have asserted the high-spin state for all the iron ions in the two families of oxides, the hypothesis of intermediate or low-spin iron states can be discarded. As a consequence, the C′ fitted IS values surely correspond to iron sites in intermediate valence states between +3 and +4.

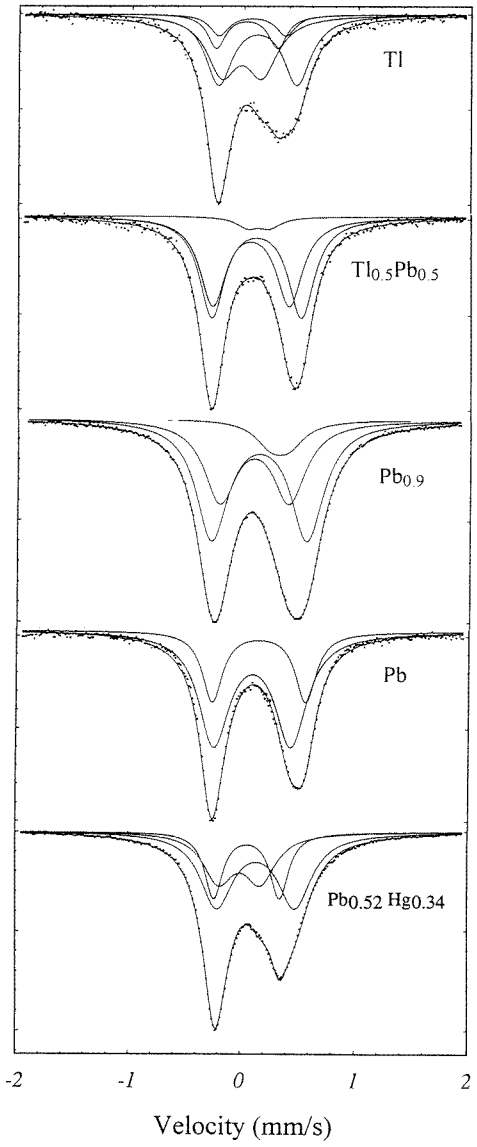

Figure 5. Mössbauer spectra at 293 K of the (Tl, Pb, Hg)$Sr_4Fe_2O_9$ series.

In such a way, the correlation of the 4.2 K and RT Mössbauer results would allow us to establish precisely these intermediate-valence states for the C′ sites and the related electron transfer mechanisms.

For $TlSr_3Fe_2O_8$, besides two A′ (Fe^{3+}) sites (IS = 0.29 and 0.31 mm s^{-1}), a third contribution is observed whose IS = 0.01 mm s^{-1} is typical of Fe^{4+} ($S = 2$). Its intensity (34%) is equal to that of the B site at 4.2 K (35%). This allows us to assert that the B sites, observed in low-temperature spectra, probably correspond to Fe^{4+}.

Note that the single Fe^{3+} line (site D) at 4.2 K is also evidenced in the RT spectra when its relative intensity at low temperature is greater than 10%. In the cases where two

localized A'_1 and A'_2 (Fe^{3+}) sites are observed with different QS values, EFG calculations have been performed in order to understand the existence of these two iron sites correlated to their local environment. The existence of these sites was previously explained on the basis of an apical $O_{(2)}$ oxygen displacement in the FeO_6 octahedron [2, 3, 5, 6].

3.3. Electronic iron states deduced from the 4.2 K and RT Mössbauer spectra

As already indicated, the A_1 and A_2 sites observed at 4.2 K as well as the A'_1 and A'_2 sites observed at 293 K can be assigned to high-spin Fe^{3+}. In the following paragraph particular attention is paid to the problem concerning the origin of the C′ sites at RT for which IS values are intermediate between those of localized Fe^{3+} and Fe^{4+}.

From the examination of Mössbauer data (tables 1 and 2) and chemical analysis measurements (table 3), it appears that, in both O_8 and O_9 series, the C′ valence state depends on the oxygen content and also on the nature, i.e. the mean charge, of the $5d^{10}$ cations (Tl, Hg, Pb). This leads us to perform a detailed analysis of the results obtained at low and room temperatures for each composition.

3.3.1. O_8 compounds At 293 K, such a C′ iron site is not present for the $TlSr_3Fe_2O_8$ phase which corresponds to a charge on the A site equal to +2.85 (table 1). In contrast, for the $Tl_{0.5}Pb_{0.5}Sr_3Fe_2O_8$ phase, corresponding to a higher A charge (+3.5), one observes two C′ sites for which the IS values ($IS(C'_1) = 0.18$ mm s^{-1} and $IS(C'_2) = 0.09$ mm s^{-1}) are intermediate between the values expected for Fe^{3+} and Fe^{4+}. As a result, we assign a unique '$m+$' charge to the C'_1 site and a unique '$n+$' charge to the C'_2 site, with $3 < m < n < 4$. Note that the relative intensity of the Fe^{3+} species ($A_1 + A_2 = 72\%$) at 4.2 K decreases to 49% at 293 K. Hence, one can propose the following electron transfer mechanism from 4.2 K to RT :

$$\alpha Fe^{3+} + \beta Fe^{4+} \Rightarrow \alpha' Fe^{m+} + \beta' Fe^{n+} \tag{1}$$

with $\alpha + \beta = \alpha' + \beta'$ and $3\alpha + 4\beta = m\alpha' + n\beta'$.

For this type (1) process it should be considered that the electron transfer between Fe^{3+} and Fe^{4+} sites is not complete.

3.3.2. O_9 compounds. At 293 K, two types of electron delocalization can be considered, depending upon the charge of the $5d^{10}$ cations. In the cases of $TlSr_4Fe_2O_9$ and $Pb_{0.52}Hg_{0.34}Sr_4Fe_2O_9$ with weak A charge (< +3), the IS values of C'_1 and C'_2 (table 2) lead to $m+$ and $n+$ valence states as for $Tl_{0.5}Pb_{0.5}Sr_3Fe_2O_8$, following a similar electron transfer mechanism (type (1)).

For the two other compounds of this family, $Tl_{0.5}Pb_{0.5}Sr_4Fe_2O_9$ and $Pb_{0.9}Sr_4Fe_2O_9$, whose A charge is larger ($\geqslant +3.5$), only one C′ site is present at 293 K. Moreover, in both oxides, the C′ intensity (45% and 41% respectively) is about twice the Fe^{4+} ratio observed at 4.2 K (26% and 21% respectively); this suggests the following disproportionation process between 4.2 K and RT:

$$Fe^{3+} + Fe^{4+} \Rightarrow 2Fe^{3.5+}. \tag{2}$$

Contrary to the type (1) mechanism, this type (2) electron transfer is total between Fe^{3+} and Fe^{4+} sites.

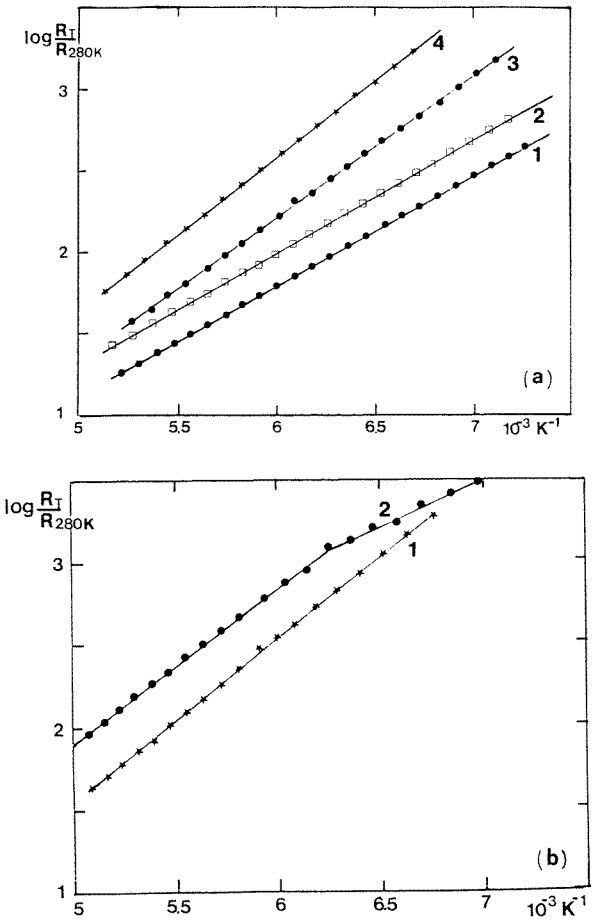

Figure 6. Plots of log $(R_T/R_{280\ \mathrm{K}})$ versus $1/T$ for (a) O_9 series: 1, $Pb_{0.9}Sr_4Fe_2O_9$; 2, $Tl_{0.5}Pb_{0.5}Sr_4Fe_2O_9$; 3, $TlSr_4Fe_2O_9$; 4, $Pb_{0.52}Hg_{0.34}Sr_4Fe_2O_{8.58}$ (b) O_8 series: 1, $TlSr_3Fe_2O_8$; 2, $Tl_{0.5}Pb_{0.5}Sr_3Fe_2O_8$.

3.4. Behaviour of the 'O₈' and 'O₉' oxides versus temperature

As shown here above, two charge transfer mechanisms (types (1) and (2)) can be suggested and correlated with the mean charge of the A cation. In a same way, one can expect that such a process would also influence the electronic conductivity of the materials. It can indeed be seen (figures 6(a) and (b)) that these oxides exhibit a linear variation of $\log(R_T/R_{280\ \mathrm{K}})$ versus $1/T$ typical of a semiconducting behaviour. Note that for $Tl_{0.5}Pb_{0.5}Sr_3Fe_2O_8$ a slope change appears at about 160 K (figure 6(b)).

In each family, when the A charge increases, the activation energy E_a value decreases (table 4), involving a higher electronic conductivity. As suggested for the layered superconducting cuprates, the $[(Tl, Pb)O]_\infty$ layers may play the role of hole reservoirs, increasing the charge of iron in the A sites; moreover replacing Tl(III) by Pb(IV) generates a change of the coordination of these cations within the rock salt layers, and consequently induces a displacement of the $O_{(2)}$ position. As a result, the apical Fe–$O_{(2)}$ distance is increased as previously demonstrated from X-ray, neutron diffraction and from Mössbauer

Table 4. Activation energy E_a determined from $\log(R_T/R_{280\ K}) = f(1/T)$ curves. The mean A charges are deduced from EDS analysis and X-ray or neutron diffraction studies.

Compound	Mean A charge	E_a (eV)
$TlSr_3Fe_2O_8$	+2.85	0.198
$Tl_{0.5}Pb_{0.5}Sr_3Fe_2O_8$	+3.50	0.182 for $T > 160$ K 0.115 for $T < 160$ K
$TlSr_4Fe_2O_9$	+2.94	0.177
$Pb_{0.52}Hg_{0.34}Sr_4Fe_2O_9$	+2.76	0.204
$Tl_{0.5}Pb_{0.5}Sr_4Fe_2O_9$	+3.50	0.140
$Pb_{0.9}Sr_4Fe_2O_9$	+3.60	0.137

spectrometry measurements correlated with EFG calculations [2, 3]. This displacement of $O_{(2)}$ further away from Fe probably reinforces the electronic exchange in the basal $[FeO_2]_\infty$ planes and increases the conductivity of the material.

The observed E_a values are characteristic of a thermally activated electronic hopping process between $Fe^{3+}$and Fe^{4+} over b_{1g} orbitals.

At this stage, in order to check the effect of the temperature on these exchange mechanisms, we have performed a Mössbauer study at various temperatures for the mixed composition '$Tl_{0.5}Pb_{0.5}$' in both O_8 and O_9 series. At 20 K, the spectrum of $Tl_{0.5}Pb_{0.5}Sr_4Fe_2O_9$ is magnetic (figure 7(c)) with the fitted Fe^{3+}:Fe^{4+} ratio close to that obtained for the 4.2 K spectrum, whereas all iron ions are paramagnetic at 77 K (figure 7(b)). Moreover, the fit of the Mössbauer spectrum shows that, at this temperature, the electron hopping is already visible, characterized by the presence of two Fe^{m+} and Fe^{n+} sites whose IS values are equal to 0.22 and 0.19 mm s^{-1} respectively (table 2). This suggests that the electron delocalization starts at a temperature T_d ranging between 20 and 77 K. The sum of the Fe^{m+} and Fe^{n+} site intensities ($C'_1 + C'_2 = 47\%$) is very close to that of the $Fe^{3.5+}$ species (45%) obtained at 293 K. Therefore, the thermal evolution of the Mössbauer results for this phase can be explained on the basis of a type (1) charge transfer between 4.2 K and 77 K and of a type (2) transfer at higher temperature ($T > 293$ K).

In contrast, the Mössbauer spectrum at 77 K of the mixed $Tl_{0.5}Pb_{0.5}Sr_3Fe_2O_8$ phase (figure 7(a)) shows that the sample is still in a magnetic transition zone. However, the spectrum registered at 150 K (figure 8) becomes entirely paramagnetic, but iron ions still exhibit localized Fe^{3+} and Fe^{4+} valence states (table 1). The relative intensities agree with the formulation. On the other hand, one observes a visible change in the paramagnetic Mössbauer spectra when $T \geqslant 180$ K (figure 8). As can be seen in table 1, one has indeed to introduce two C′ sites corresponding to Fe^{m+} and Fe^{n+} valence states to fit the Mössbauer spectra recorded at 180, 210, 240 and 293 K. These results suggest that the electron delocalization could be under way at 180 K following the type (1) process.

Moreover, Mössbauer spectra recorded at high temperatures ($T > 293$ K) (figure 8) have allowed us to demonstrate the type (2) mechanism at $T = 400$ K. The fits of the 400 K spectrum (table 1) reveal indeed the presence of two principal components with IS = 0.18 and 0.11 mm s^{-1} instead of three (1A′ + 2C′) sites at 293 K. The intensity of the IS = 0.18 mm s^{-1} component is identical to that observed for the A′ site at RT. This confirms the Fe^{3+} charge for this site. Furthermore, we can note that this IS value well agrees with the second-order Doppler effect on the chemical Fe^{3+} isomer shift as can be observed in the IS = $f(T)$ curve (figure 9). Therefore, it seems realistic to attribute the second component with IS = 0.11 mm s^{-1} to an iron charge close to +3.5.

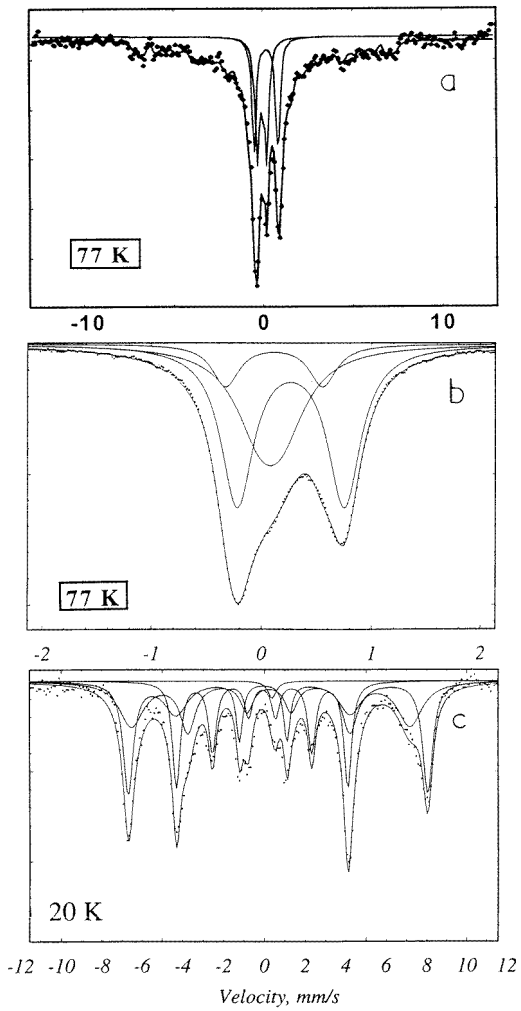

Figure 7. Mössbauer spectra at 77 K of $Tl_{0.5}Pb_{0.5}Sr_3Fe_2O_8$ (a), $Tl_{0.5}Pb_{0.5}Sr_4Fe_2O_9$ (b), and at 20 K for $Tl_{0.5}Pb_{0.5}Sr_4Fe_2O_9$ (c).

These results lead us to conclude that for both '$Tl_{0.5}Pb_{0.5}$' compounds, the two types of delocalization should not be ascribed to two distinct mechanisms but that they can be considered as two aspects of the same dynamical electron exchange process. The existence of two delocalized $(m+)$ and $(n+)$ charges or of only one 'averaged' $3.5+$ one is strongly dependent on the relative magnitude of the electron hopping frequency compared to that of the characteristic Mössbauer frequency. For a fast electron transfer, the hopping frequency ν is indeed higher than the nuclear Larmor frequency ν_L ($\nu_L \approx 5.1 \times 10^8$ Hz for ^{57}Fe); the Mössbauer spectroscopy can evidence only a mean situation corresponding to the observation of $3.5+$ charge for C′ sites (type (2)). In contrast, if $\nu \leqslant \nu_L$, the two separate $m+$ and $n+$ valence states (type (1)) become observable simultaneously on the Mössbauer spectra. Therefore, an increase of the temperature would lead to an evolution from $(Fe^{m+} + Fe^{n+})$ to $Fe^{3.5+}$ iron species.

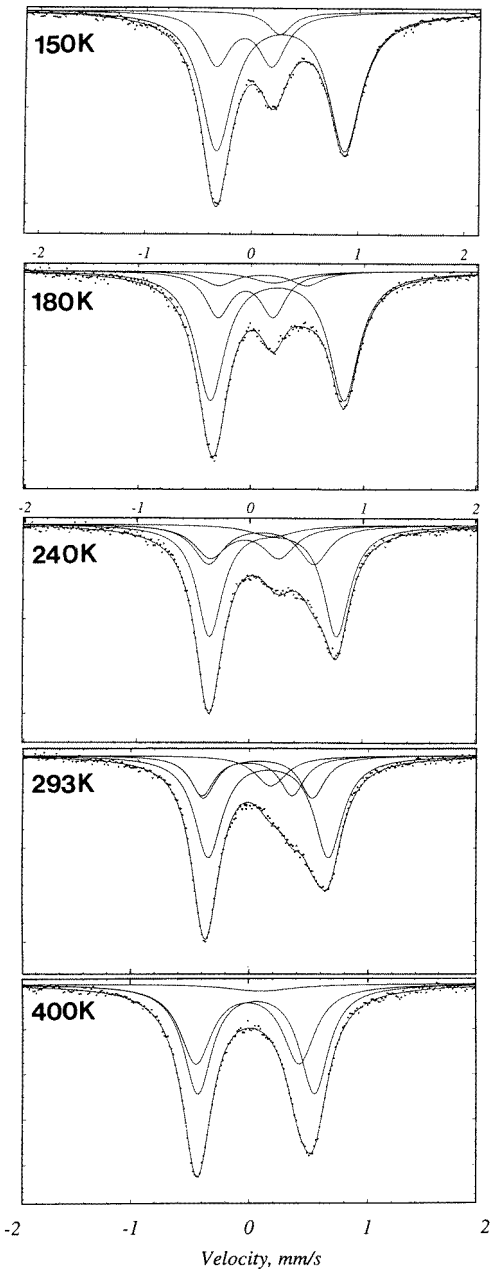

Figure 8. Thermal evolution of the Mössbauer spectra for the $Tl_{0.5}Pb_{0.5}Sr_3Fe_2O_8$ compound.

As shown from the Mössbauer room-temperature results, in each series of oxides, if one considers the situation at a given temperature T, the higher the A charge, the faster the electron hopping. This can be predicted according to [14, 15] by the relation giving the hopping frequency, expressed as

$$\nu(T) = \nu_0 f(T) \exp(-E_{ah}/kT)$$

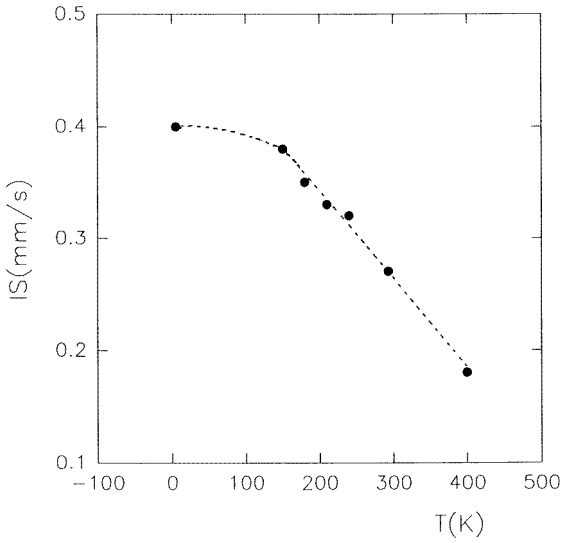

Figure 9. Thermal evolution of the IS value for the main Fe^{3+} site (A or A′) in $Tl_{0.5}Pb_{0.5}Sr_3Fe_2O_8$.

where ν_0 is the lattice vibrational frequency of the sample, $f(T)$ the probability of hopping between two iron sites and E_{ah} the activation energy of the electronic process.

Assuming that ν_0 is not strongly dependent on the A charge and taking account of the fact that E_{ah} decreases and $f(T)$ increases as the A charge increases, since the conduction in the $[FeO_2]_\infty$ planes is enhanced, it is easy to show that $\nu(T)$ increases with A charge.

Consequently, the higher the A charge, the lower the T_d temperature for which the hopping process begins. This conclusion is in agreement with the Mössbauer observations. For instance, in the O_8 family: $T_d \approx 180$ K for A = 3.5+, while for A < 3+, $T_d > 300$ K are observed.

Considering simultaneously the above thermal evolutions of the Mössbauer results for $Tl_{0.5}Pb_{0.5}Sr_4Fe_2O_9$ and $Tl_{0.5}Pb_{0.5}Sr_3Fe_2O_8$ oxides, it appears that, for the same A cations, the electron delocalization begins at a lower T_d temperature in the O_9 compound than in the O_8 counterpart (20 K < T_d < 77 K for O_9 and $T_d \approx 180$ K for O_8 respectively). This T_d displacement may be correlated to the difference of the structures (figure 1). O_8 oxide structure exhibits indeed FeO_6 octahedral double layers leading to a quasi-three-dimensional behaviour, whereas in the O_9 phase, single octahedral FeO_6 layers confer to the structure a two-dimensional behaviour which favours the electron exchange within the basal planes.

The dimensionality of the structure seems also to play a role in the magnetic behaviour of the compounds. As an example, figure 10 shows the $\chi_M^{-1} = f(T)$ curves of the two oxides $TlSr_3Fe_2O_8$ and $TlSr_4Fe_2O_9$, representative of the O_8 and O_9 families. Antiferromagnetic interactions appear to prevail in both of them but we can note that the extrapolated paramagnetic Curie temperature is much more negative for the O_8 phase than for the O_9 one (table 5).

Using the Fe^{4+}:Fe^{3+} ratio (= 35:65% for both compounds) determined at 4.2 K by Mössbauer spectroscopy, and taking for the Fe^{3+} and Fe^{4+} species the high-spin magnetic moments ($\mu_{Fe^{3+}} = 5.9\mu_B$; $\mu_{Fe^{4+}} = 4.9\mu_B$), the molar Curie constant C_{cal} values are

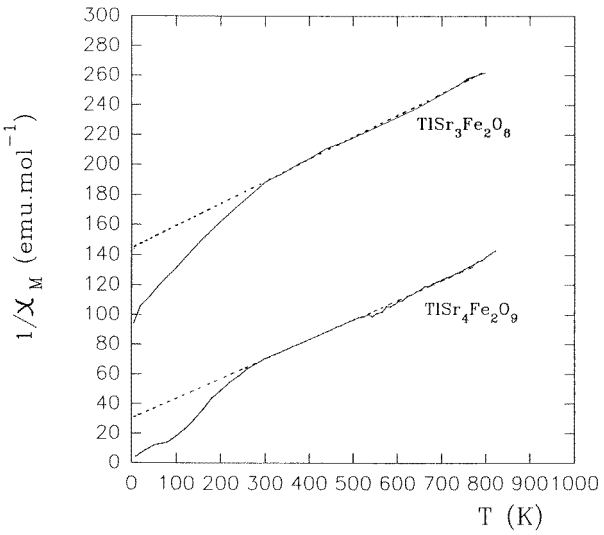

Figure 10. Reciprocal molar magnetic susceptibility versus temperature of the $TlSr_3Fe_2O_8$ and $TlSr_4Fe_2O_9$ compounds.

Table 5. Magnetic data of $TlSr_4Fe_2O_9$ and $TlSr_3Fe_2O_8$.

Compound	$\Theta_p(\mp 5$ K)	$T_N(\mp 5$ K)	C_{cal}	C_{obs}
$TlSr_4Fe_2O_9$	−228	80	7.70	7.74
$TSr_3Fe_2O_8$	−920	<4	7.79	7.26

estimated to be 7.79 and 7.70 for $TlSr_3Fe_2O_8$ and $TlSr_4Fe_2O_9$ respectively. One can note that for the O_8 phase the experimental C_{obs} value (7.26) deduced in the Curie–Weiss range ($T > 300$ K) is lower than the C_{cal} one (table 5). On the other hand, the value observed for $TlSr_4Fe_2O_9$, ($C_{obs} = 7.74$) is in good agreement with the corresponding C_{cal} value.

4. Concluding remarks

The Mössbauer study combined with the electron transport properties and magnetic susceptibility data clearly demonstrates three important features for the layered $ASr_3Fe_2O_8$ and $ASr_4Fe_2O_9$ ferrites. The first important one deals with the fact that all of them exhibit a mixture of localized Fe^{3+} and Fe^{4+} species at low temperature. Second, it is shown for the first time that an electron transfer between Fe^{3+} and Fe^{4+} takes place, leading in the gap of the Mössbauer window to the observation of either two different intermediate $m+$ and $n+$ charges or only one averaged $3.5+$ valence state. This is dependent on the magnitude of the electron hopping frequency which, in turn, is related to the mean charge of the A cations. The third interesting point deals with the two-dimensional character of the 'O_9' structure that enhances the electron exchange within the basal $(FeO_2)_\infty$ planes.

Acknowledgments

The authors would like to thank Professor M Hervieu for performing the EDS analysis and Drs V Caignaert and A Maignan for their help in neutron diffraction and electronic conductivity measurements.

References

[1] Lucas S, Groult D, Nguyen N, Michel C, Hervieu M and Raveau B 1993 *J. Solid State Chem.* **102** 20
[2] Caignaert V, Daniel Ph, Nguyen N, Ducouret A, Groult D and Raveau B 1994 *J. Solid State Chem* **112** 126
[3] Daniel Ph, Barbey L, Groult D, Nguyen N, Van Tendeloo G and Raveau B 1994 *Eur. J. Solid State Inorg. Chem.* **31** 235
[4] Nguyen N, Daniel Ph, Groult D, Raveau B and Grenèche J M 1996 *Mater. Chem. Phys.* **45** 33
[5] Daniel Ph, Barbey L, Nguyen N, Ducouret A, Groult D and Raveau B 1994 *J. Phys. Chem. Solids* **55** 795
[6] Nguyen N, Groult D, Caignaert V, Ducouret A and Raveau B 1996 *Physica* B accepted for publication
[7] Martin C, Maignan A, Huve M, Hervieu M, Michel C and Raveau B 1991 *Physica* C **179** 1
[8] Morosin B, Ginley D S, Hlava P F, Carr M J, Baughman R J, Schirber J E, Venturini E L and Kwak J F 1988 *Physica* C **152** 413
[9] Parise J B, Gai P L, Subramanian M A, Gopalakrishnan J and Sleight A W 1989 *Physica* C **159** 245
[10] Seguelong T, Maestro P, Grenier J C, Fournes L and Pouchard M 1995 *Physica* B **215** 427
[11] Teillet J and Varret F unpublished Mosfit program
[12] Kawasaki S, Takano M and Takeda Y 1996 *J. Solid State Chem.* **121** 174
[13] Greenwood N N and Gibb T C 1971 *Mössbauer Spectroscopy* (London: Chapman and Hall) p 91
[14] Lotgering F K and Van Diepen A M 1977 *J. Phys. Chem. Solids* **38** 565
[15] Gerardin R, Ramdani A, Gleitzer C, Gillot B and Durand B 1985 *J. Solid State Chem.* **57** 215